JOURNAL OF MATERIALS SCIENCE 21 (1986) 1837–1852

Review
Influence of grain size on the mechanical behaviour of some high strength materials

A. LASALMONIE
Direction des Matériaux, ONERA, Av Division Leclerc, 92320 Chatillon, France
J. L. STRUDEL
Centre des Matériaux, Ecole des Mines de Paris, BP 87, 91003 Evry, France

Combining in an additive or synergetic manner the most potent strengthening mechanisms available in an alloy is the art of the metallurgist. The various models proposed in the literature in order to interpret the Hall–Petch relation are critically reviewed by comparison with experimental data. The pile-up models and the work hardening theories must include the inner structure of the grain in the case of alloys hardened by a second phase. Similarly, the properties and structure of the grain boundaries are influenced by impurities or the presence of particles. Ultra-fine grain sizes can provide ductility to high strength materials when surface preparation eliminates microcracks.

In steady-state creep equations, introducing the influence of grain size in complex alloys by incorporating the Hall–Petch stress as one component of the internal stress helps in rationalizing the existence of an optimal grain size where creep resistance is maximized. Slower crack growth rates can be obtained by controlling the grain boundary structure as well as grain size. Fatigue tests at room temperature clearly point out the interest of small grain sizes for reducing crack initiation, usually associated, however, with lower propagation threshold and somewhat faster growth rates.

1. Introduction

The influence of grain size on mechanical properties is complex since the grain boundaries may either act as obstacles to dislocation slip (strengthening effect) or provide a positive contribution to the deformation of the material (softening effect). The importance of these two opposite effects depends on temperature as illustrated by the work of Kutumba Rao *et al.* [1] (Fig. 1).

The cross-over temperature, T_c, is not a well-defined physical parameter since, for a given alloy, it depends on the microstructure and on the deformation rate. The general trend is for T_c to increase when the yield stress increases. For instance Fig. 2 is taken from results of Gibbons and Hopkins [2] on Ni-based alloys containing various amounts of the strengthening, γ', phase: at 750° C the solid solution with its low yield stress is still in the $T < T_c$ domain, whereas the strongest alloys (19% and 31% γ') are well above T_c. In all cases T_c is generally higher than $0.5\,T_m$, where T_m is the melting temperature.

We shall study successively the two domains. Below T_c we will be concerned mainly with the Hall–Petch law. We shall compare the experimental results and the various theories and show that there are good theoretical reasons for the deviation from the Hall–Petch law at very small grain sizes.

The second part of this paper will be devoted to high temperature plasticity where the contribution of the grain boundary deformation becomes important.

The third part will be concerned with the influence of grain size on the mechanical behaviour during cyclic deformation at room temperature. The discussion will be focused frequently on nickel and Ni-based alloys (solid solutions and γ–γ' superalloys). When experimental results are available we shall examine whether the behaviour of materials with ultra-fine grain sizes is the same as that of alloys with large grains. With the progress of rapid solidification techniques, metallic alloys with grain sizes in the submicron range are now manufactured which have a growing technological importance [3].

2. Deformation at low temperature (the Hall–Petch law)

2.1. The models

In most cases the flow stress at low temperature σ depends on the grain size according to the Hall–Petch relationship [4, 5]:

$$\sigma = \sigma_0 + kd^{-1/2} \quad (1)$$

where σ_0 is a friction stress and k is the Hall–Petch coefficient. Many of the models elaborated in order to interpret this phenomenological equation, have been based on dislocation theory. They have been reviewed by Li and Chou [6] and a detailed account of the

0022–2461/86 $03.00 + .12

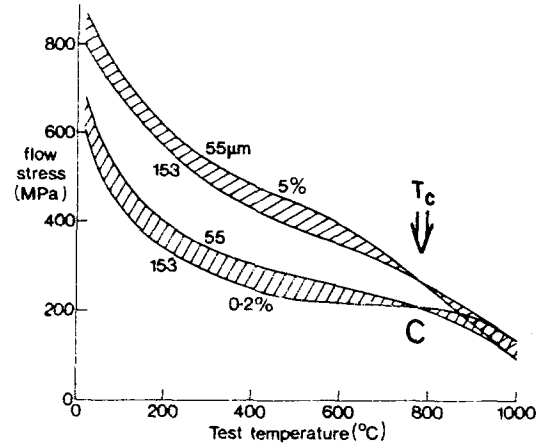

Figure 1 Influence of grain size on the flow stress at 0.2% and 5% strain in manganese stainless steel. The range of temperature is straddling the cross-over point T_c [1].

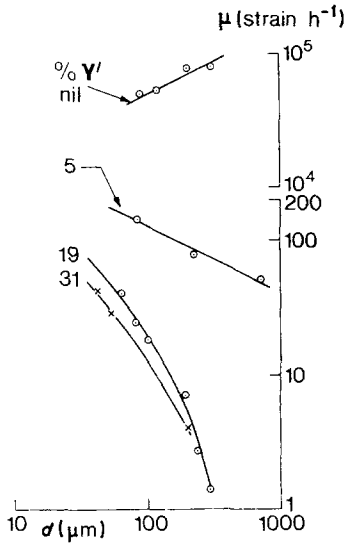

Figure 2 Influence of grain size on creep at 750° C rate in Ni–Cr based alloys with various volume fractions of γ' precipitates [2].

experimental results on steels was drawn recently by Armstrong [7].

Existing models can be classified into three broad categories. (The main equations derived from these theories are gathered in Table I; the Petch slope, k, is given as a function of the shear modulus, G.)

1. Pile-up models. The deformation propagates in the polycrystal when a critical stress τ_c is reached at the tip of the pile-ups [4, 5, 8, 9]. The initial models for the yield point were extended to describe the flow stress at strain ε (see Table I, Relations c and d [10, 11]).

2. The work-hardening theories. These are based on a linear relationship between the flow stress and the square root of the dislocation density ϱ. Ashby [12] made the distinction between two types of dislocations:

the statistical dislocations of density $\varrho_s = \varepsilon(b/\lambda)$ where λ is the average slip length and ε is the strain amplitude.

the geometrically necessary dislocation of density, $\varrho_G = \varepsilon/(4bd)$.

Coefficient k in Relation 1 is then proportional to $\varepsilon^{1/2}$ (Relation e in Table I), it is also a function of ε through λ.

For Thompson *et al.* [13] ϱ_s is randomly spread over the entire grain whereas ϱ_G is more concentrated in the vicinity of the boundaries; with this heterogeneous distribution of dislocations the expression of the flow stress is more complicated (Relation f in Table I). It reduces to Equation 1 only if $\lambda = d$.

TABLE I Various attempts to rationalize the Hall–Petch relation

Model	Conditions	Equations	
Pile-up models	At the yield stress (YS) [4, 5, 7, 9] simple-pile-ups of infinitely straight mixed dislocations	$k \simeq 0.7\left(\frac{\tau_c}{G}\right)^{1/2} G(b)^{1/2}$	(a)
	simple pile-ups of loops	$k \simeq 2\left(\frac{\tau_c}{G}\right)^{1/2} G(b)^{1/2}$	(b)
	(τ_c is the critical YS of the grain boundary)		
	At a given strain ε [10, 11]		
		$\sigma = \sigma_0 + \chi\varepsilon$	(c)
		$k = k_0 + \beta\varepsilon^{1/2}$	(d)
Work hardening	Ashby's model [12]	$k = \alpha G(b)^{1/2}\left(\frac{1}{4} + \frac{d}{\lambda}\right)^{1/2}\varepsilon^{1/2}$	(e)
	Thompson *et al.* [13]	$\sigma = \sigma_0 + \left(1 - \frac{\lambda}{d}\right)\frac{k_1}{\lambda} + \frac{\lambda}{d}\frac{k_2}{d^{1/2}}$	(f)
Composite	Thompson *et al.* [13] Equation f		
	GB source model: Li [14, 15]	$k = 0.4\,Gb(3\varrho_1)^{1/2}$	(g)
		$k = 0.4\,Gb\left(\frac{8\varrho_D}{\pi}\right)^{1/2}$	(g′)
	Core-mantle models: Kocks [16]	$\tau = \tau_0\left[1 + \frac{4t}{d}\left(\frac{\tau_B}{\tau_0} - 1\right)\right]$	(h)

τ_0 = flow stress of the grain interior (core)
τ_B = flow stress of the grain boundary region (mantle)
t = thickness of the mantle which depends on ε but on neither τ_0 nor τ_B.

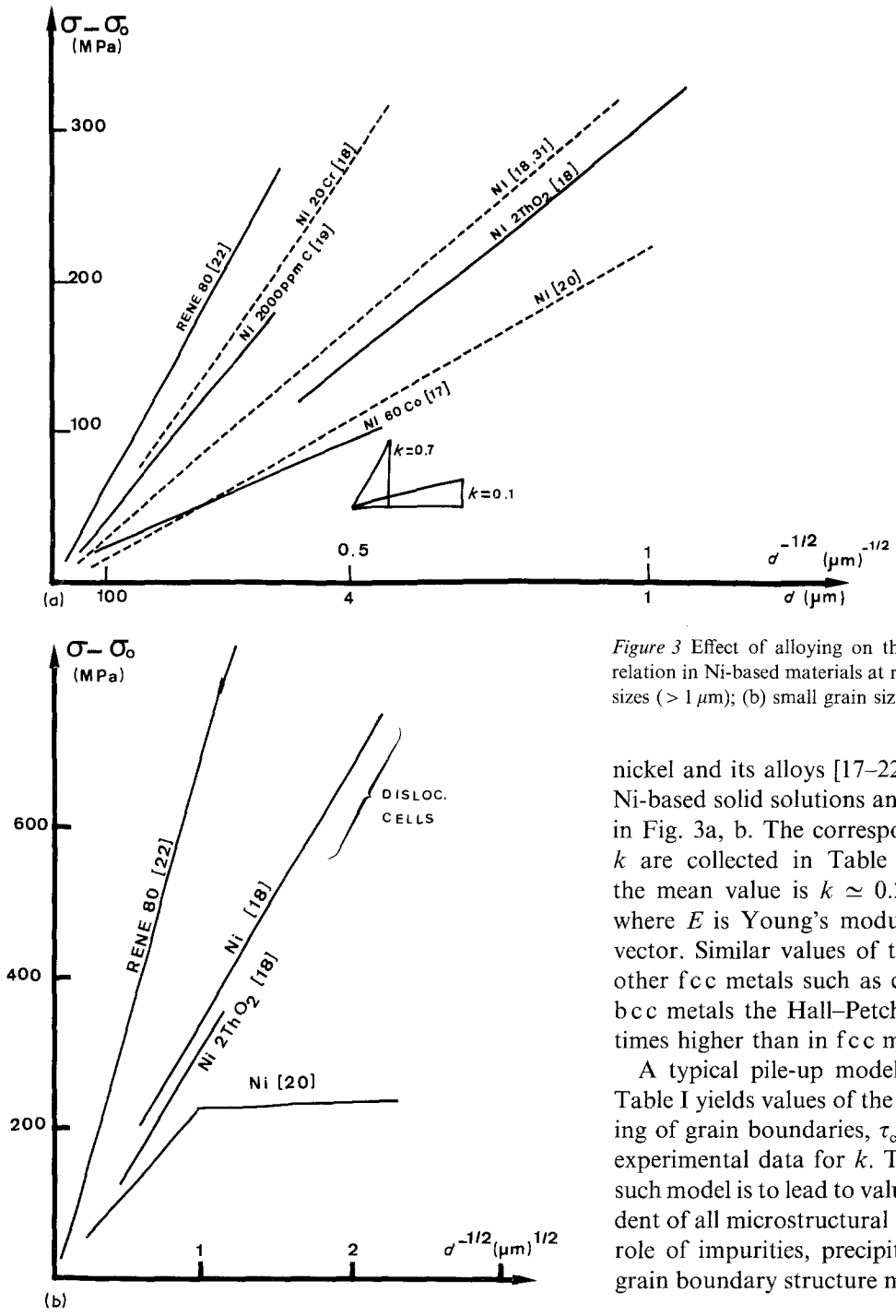

Figure 3 Effect of alloying on the k constant of the Hall–Petch relation in Ni-based materials at room temperature: (a) large grain sizes ($> 1\ \mu m$); (b) small grain sizes.

3. Theories based on the intrinsic properties of the grain boundary interface. In the first group we find the grain boundary source models. Coefficient k is then a function of the density of grain boundary sources, $\varrho_{\parallel}$, [14] or of the total length of dislocations emitted per unit area of grain boundary, ϱ_D [15].

In a second group the polycrystal is described as a composite material where the interior of the grain has a flow stress τ_G, whereas an area of thickness t, along the boundaries has a flow stress τ_B [16]. The Hall–Petch relation does not hold in this case since the yield stress is a function of d^{-1}. This relation is expected to be valid at very small grain sizes where $t \simeq d$.

2.2. Comparison with experimental results

2.2.1. The Hall–Petch slope for the yield stress

The Hall–Petch law is quite generally verified by nickel and its alloys [17–22]. Results for pure nickel, Ni-based solid solutions and superalloys are sketched in Fig. 3a, b. The corresponding values of the slope k are collected in Table II. For unalloyed nickel the mean value is $k \simeq 0.25\,MN\,m^{-3/2} \simeq E(b)^{1/2}/15$, where E is Young's modulus and b is the Burger's vector. Similar values of the k/E ratio are found in other fcc metals such as copper and aluminium. In bcc metals the Hall–Petch slope is generally 2 to 3 times higher than in fcc metals [10].

A typical pile-up model such as Expression a in Table I yields values of the critical stress for the yielding of grain boundaries, $\tau_c = G/100$, when using the experimental data for k. The major short-coming of such model is to lead to values of τ_c which are independent of all microstructural aspects of the material: the role of impurities, precipitates, particles, strain and grain boundary structure must be taken into account.

2.2.2. The influence of composition

In the case of alloys, it is difficult to separate the influence of grain size from that of other microstructural features: texture, size and volume fraction of precipitates. The structural parameters affect σ_0 quite directly. However, a careful examination of Table II indicates that k also increases with the strength of the alloy ($k = 0.7$ for the γ' strengthened alloy René 80) (Fig. 3). From Fig. 3a, it seems that cobalt does not increase k whereas carbon and chromium have a large strengthening influence.

The effect of the spread in the grain size distribution is usually not considered in most studies. The shape of the grain size histogram can be an important parameter [27], either when the grains are flat or elongated (pancake structures) or when there is a wide spread of sizes around the value of the mean diameter: necklace structures in γ–γ' superalloys for instance. It is also clear that grain boundary hardening can be

TABLE II Parameters of the Hall–Petch relation. Values at 300 K

Composition	Grain size (μm)	k ($MNm^{-3/2}$)	σ_0 (MPa)	Reference
Ni	1–130	0.16	22	[23]
Ni, 1–22 ppm S	100–1000	0.3–0.6	30	[24]
Ni, 20–810 ppm C	15–100	0.15–0.25	15–30	[17]
Ni, 600–2000 ppm C	10–250	0.24–0.6	15–25	[19]
Ni, 10 ppm C	0.2–200	0.35	< 10	[25]
Ni, 60 Co, 70–590 ppm C	5–100	0.25–0.30	25–50	[17]
Ni–2 ThO_2	0.2–50	0.3	150	[25]
René 80	0.5–17	0.7	700	[22]
Ni–Al	5–120	0.16	150	[26]

outweighed by the presence of other strong interfaces. In two-phase lamellar alloys such as Ni/Nb_3Nb, the spacing between incoherent interfaces becomes much smaller than the grain diameter. The Hall–Petch law then correlates the yield stress of the composite material with the distance between interfaces.

Recently Werner and Stüwe [28] examined the case of dual-phase brass with various grain size distributions and proportions. They reported that the plastic flow of these α–β mixtures was influenced by the density of grain and phase boundaries. In structures where the preferentially deformed phase is of high contiguity, grain boundaries of this phase act as dislocation obstacles, whereas the phase boundaries act as the predominant dislocation obstacles when the preferentially deformed phase is of low contiguity. The measured value of the Hall–Petch coefficient, k, for the dual-phase material is not very sensitive to the proportion of the two phases but more to their contiguity and is directly related to $k^{\alpha-\beta}$, characterizing the high strength of the α–β interphase, rather than to $k^{\alpha-\alpha}$ or $k^{\beta-\beta}$, characterizing, respectively, the grain boundaries of each phase which are much weaker.

In precipitation and/or particle hardened alloys, the effect of the grain size may become secondary as the density of dislocation barriers and sources may be drastically increased. This was first established by Wert [29] in Alloy 7075 and confirmed by the work of Kim and Griffith [30] on another powder metallurgy (PM) aluminium alloy (Alloy 7091) containing both oxide particles and Co_2Al_9 precipitates whose sizes are controlled by heat treatment. If in the underaged condition (UA in Fig. 4) the Hall–Petch effect is observed for 2 to 50 μm size grains, it is the contrary for the peak-aged (PA) and overaged (OA) states, the YS is, then, grain-size independent from 8 to 1000 μm.

By introducing various amounts of aluminium into a Cu-based alloy Higo *et al.* [27] could modify the stacking fault energy (SFE) of the material and correlate more planar slip, associated with lower SFE, with higher values of the Hall–Petch coefficient (Fig. 5).

2.2.3. Extension of the Hall–Petch law to larger strains

As Meakin and Petch [11] anticipated, k is often found to increase with ε. An example of the $k(\varepsilon)$ variation is given on Fig. 6. In pure aluminium and copper, non-monotonic variations were reported by Hansen [32] who also introduced the effect of temperature and of Al_2O_3 particles. The study of $k(\varepsilon)$ is a good test for the yield stress model and for the work-hardening theories.

In Fig. 6, for pure nickel $k = A(\varepsilon)^{1/2}$, in agreement with Expressions d and e of Table I. On the contrary NiCo alloys do not appear to exhibit parabolic hardening. In fact, it seems that a full account of the

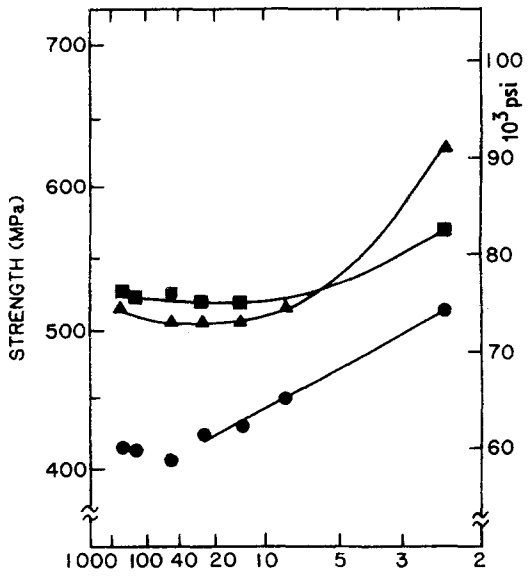

Figure 4 The variation of yield strength (YS) at 300 K for three different ageing conditions in Al-based PM 7091 alloy with average grain size, d [30]. (●) UA (121° C/2 h), (▲) PA (121° C/24 h), (■) OA (PA + 163° C/4 h).

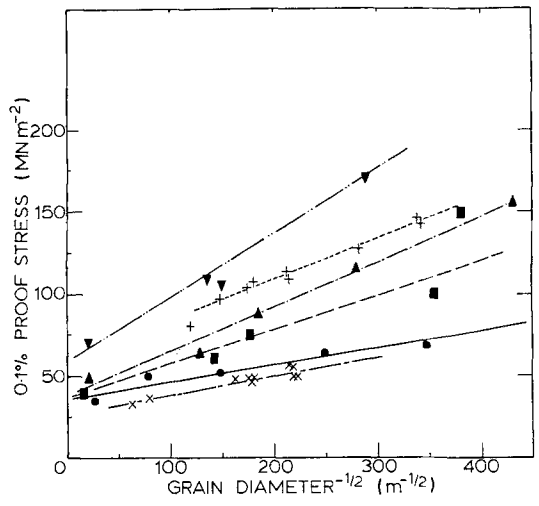

Figure 5 Variation of 0.1% proof stress with grain size in some Cu-based alloys at room temperature. Effect of SFE [31]. (●) Cu, $\sigma_y = 36 + 0.104d^{-1/2}$, (■) Cu–2Al, $\sigma_y = 36 + 0.21d^{-1/2}$, (▲) Cu–4Al, $\sigma_y = 38 + 0.27d^{-1/2}$, (▼) Cu–8Al, $\sigma_y = 59 + 0.40d^{-1/2}$, (x) Cu [10], (+) Cu–39 Zn [10].

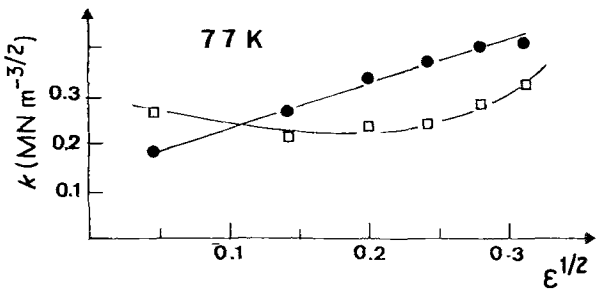

Figure 6 Variation of the Hall–Petch slope with strain in pure nickel and Ni–60 Co with 200 ppm C [17]. (●) Ni, (□) Ni–60 Co.

strain effect must include a detailed description of the dislocation distribution inside the grains. Such a model introduced by Thompson *et al.* [13] is based on the presence of statistically distributed dislocations in the grains and of geometrically necessary dislocations [12] near the boundaries. These assumptions are supported by recent observations made by Barlow *et al.* [33] in Nimonic 115. The flow stress in this model is given by Expression f in Table I, the relevant parameter being the average slip length, λ. Through an appropriate variation $\lambda(d, \varepsilon)$ (Fig. 7), Thompson [23] was able to explain the following features observed during plastic deformation in pure nickel:

(a) For small values of λ/d, i.e. for large ε and large d, Expression f, where k_1 and k_2 are two constants, reduces down to:

$$\sigma \simeq \sigma_0 + \left(1 - \frac{\lambda}{d}\right)\frac{k_1}{\lambda} \qquad (2)$$

thus the flow stres is now increasing with grain size at large strains, and the tendency for the stress–strain curves of materials with larger grain sizes (130 μm) to cross-over that of materials with smaller grain sizes (2 μm) is well interpreted (Fig. 8).

The fine substructure (pile-ups and deformation cells) which builds up in the vicinity of grain boundaries for large grain sizes due to strain incompatibility is evidenced at large strains under strain rate and temperature conditions where recovery is insignificant (Fig. 9a).

(b) For very small grain sizes ($d < 1$ μm) the $\lambda(d, \varepsilon)$ dependence is such that the flow stress is no longer influenced by the grain size, in agreement with the experimental results of Thompson (Fig. 3b). This effect will be discussed in the paragraph on ultra-fine grain sizes (see Section 2.3.).

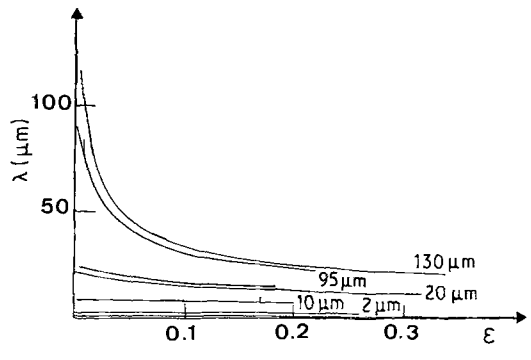

Figure 7 Calculated dependence of slip length on strain for a number of grain sizes [23].

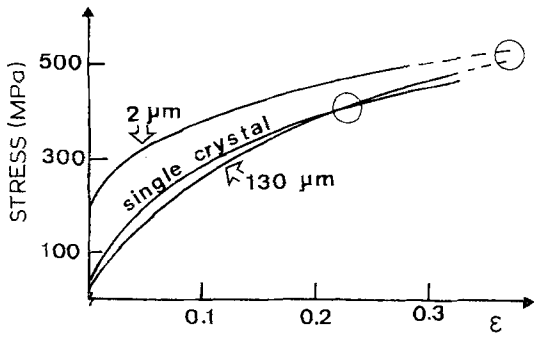

Figure 8 True stress–true strain curves for two grain sizes (2 and 130 μm) and a (1 1 1) single crystal of pure nickel [23].

2.2.4. The influence of grain boundary structure

A grain boundary may look geometrically perfect (Fig. 10a) or contain defects such as ledges or extrinsic dislocations (Fig. 10b). The number of these defects depends on several parameters which are not all independent:

(a) strain
(b) duration and temperature of annealing treatment
(c) cooling rate after annealing
(d) impurity content of the grain boundaries
(e) relative crystallographic orientation between grains
(f) grain size

Several investigations have indicated that the Hall–Petch slope, k, was sensitive to these same parameters [24, 35, 36]. TEM observations have repeatedly shown that dislocations are emitted from the ledges [37, 38]. Therefore it seems reasonable to correlate k with the density of grain boundary sources as done by Li [14, 15].

In pure nickel Venkatesh and Murr [39] were able to increase the ledge density, ϱ_L, by deforming plastically the metal prior to annealing treatment. They found (Fig. 11) that the Hall–Petch slope was a linear function of ϱ_L:

$$k = k_0(\varepsilon) + A\varrho_L \qquad (A = 12 \times 10^{-3}\ \mathrm{Nm}^{-1/2}) \quad (3)$$

Assuming that ϱ_L in Equation g, Table I, which is the source density in the grain boundaries, is in the case of ledges proportional to ϱ_L, Li's model would suggest a dependence proportional to $(\varrho_L)^{1/2}$ rather than the experimentally observed linear dependence: the ledge model, if in need of further theoretical refinement, seems to be well documented experimentally.

The crucial role played by the physico-chemical structure of the grain boundary is well illustrated by the work of Floreen and Westbrook [24]. These authors found that the addition of a few ppm of sulphur in nickel strongly modified the slope k (Fig. 12); sulphur is known to segregate to the grain boundaries of nickel thus increasing the density of grain boundary defects; this effect would explain the rapid increase of k when the sulphur content is raised from 0 to 3 ppm; above 3 ppm the decrease of k is likely to result from the inhibition of the grain boundary sources by the sulphur atoms in excess.

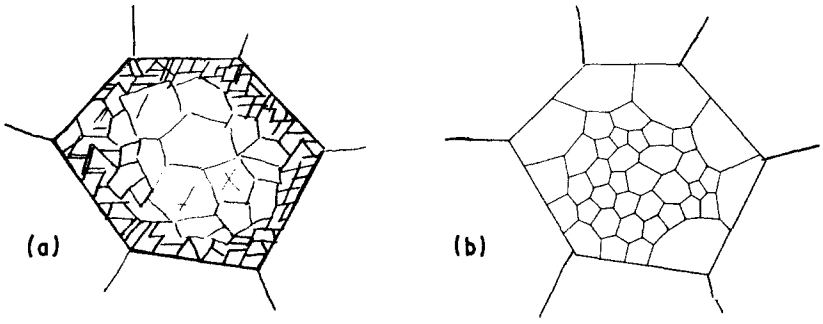

Figure 9 Intergranular substructures developing: (a) at high strain rate and/or low temperature; (b) at high temperature and/or small flow rates where recovery processes are important [34].

According to these observations the pile-up theories have to be rejected; however, other results are in contradiction with this conclusion, for example Bernstein and Rath [40] were able to vary, by heat treatment, the density of GB ledges in purified iron. They found, on the one hand that this density was only slightly sensitive to the interstitial concentration in the boundary, and on the other hand that no correlation could be found between k and the density of ledges. Thus the only firm conclusion of this is that k may depend on the boundary structure in many materials.

Among the currently used theories, only the grain boundary source models offer a simple explanation for this effect; however the GB structure can be introduced in the pile-up models through appropriate expressions of τ_c which would include some of the parameters mentioned earlier. The scarcity of detailed microstructural observations makes it difficult to select the correct model in most cases. However, it seems likely that an actual description of the polycrystal deformation should take into account both the production of dislocations at GB sources and the piling-up of dislocations against the boundaries.

2.3. The case of the ultra-fine grains

2.3.1. The models

At very small grain sizes dislocation models are meaningful only within the following limitations:

(a) Pile-ups should exist: if N is the number of dislocations in the pile-up the condition is $N \gg 1$ with

$$N \simeq \frac{\tau d}{Gb}(1 - \nu) \tag{4}$$

where τ is the shear stress and ν is Poisson's ratio. Assuming that the stress is given by the Hall–Petch relation (Equation 1) where σ_0 is neglected, we find

$$d \gg \left(\frac{Gb}{k(1 - \nu)}\right)^2 \tag{5}$$

in fcc metals where $\nu = 0.3$ and $k \simeq G(b)^{1/2}/15$ the practical limit is of the order of $d \gg 450b \simeq 0.1\,\mu$m which would still include the case of all superplastic materials.

(b) In a dislocation source model, the Hall–Petch stress must be higher than the stress, σ_s, necessary to activate a source. As the maximum length of a source is limited by the grain size, d, this condition reads $kd^{-1/2} \gg Gb/2d$ or

$$d \gg \left(\frac{Gb}{2k}\right)^2 \tag{6}$$

which yields in metallic materials $d > 60b \simeq 0.015\,\mu$m. A value difficult to reach experimentally.

(c) The Hall–Petch stress must be smaller than the theoretical yield strength $G/20$, it yields approximately $d > b$. It is not a very meaningful limitation but shows that the extrapolation of Equation 1 to the amorphous material gives a yield stress equal to the theoretical yield strength.

2.3.2. Experimental observations

We have indicated above that the pile-up theories were limited to grain sizes higher than 0.1 μm. Moreover, the strength of polycrystal is expected to be modified in the case of ultra-fine grains since the plastically deformed region of the grain adjacent to the boundary (Fig. 9a) is now involving most of the grain itself.

There are no experimental results in metallic alloys for grains smaller than 0.1 μm, the extrapolation of the Hall–Petch relation to the minimum physical grain size $d = b$ gives a yield stress $\sigma = E/15$, which is about three times higher than the observed yield stress in amorphous metals: $\sigma \simeq E/50$ [41]. If the amorphous material can be considered as a polycrystal with grain size b, a negative deviation from the Hall–Petch law is to be expected. Such a deviation was found in pure nickel by Thompson *et al.* [13], who measured a yield stress independent of the grain size below 1 μm (Fig. 3b). In Section 2.2 we saw that Thompson explained this result by an appropriate variation of the

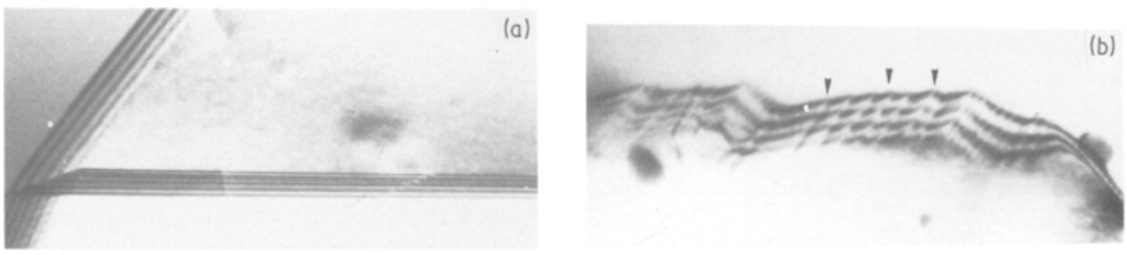

Figure 10 Aspect of grain boundaries in a Ni-based solid solution: (a) GB without imperfections; (b) GB with ledges.

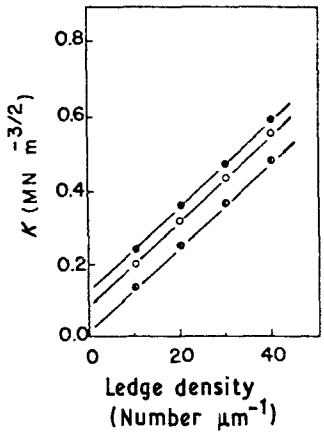

Figure 11 Graph showing the variation of Hall–Petch slope against grain boundary ledge density corresponding to: (a) 0.025%, (b) 0.1% and (c) 0.2% offset strains, respectively. Notice the slope of these plots is a constant [39].

slip length, λ, as a function of d and ε. According to the same author [20] λ can be also considered as the dislocation cell-size; these cells resulting from the rearrangement of the dislocations in the crystal play an important role in low temperature deformation.

The formation of cells decreases the elastic energy stored in the material. The difference between large-grained and fine-grained materials might correspond to the possibility of cell formation. Cells can form without difficulty in large grains, since their size and thus the slip length are a decreasing function of deformation. However, if d is smaller than the most favourable cell size the cell structure cannot form, and the slip distance is then always equal to d.

The results of Wilcox and Clauer [18, 25] on drawn nickel wires evidenced the high strengthening effect of the cell boundaries. Their results are plotted on Fig. 3b as a function of cell size, d; the cell structure was, in this case, the consequence of thermomechanical treatment; the yield stress obeys the Hall–Petch law for cell sizes smaller than 1 μm.

The low yield stresses found by Thompson below 1 μm could then be the consequence of the absence of dislocation cells; another interpretation could also be found in the fact that the fine-grained nickel was obtained by electrodeposition. In materials elaborated by this process, adjacent grains are often in twin orientation, this special type of grain boundary ($\Sigma = 3$) might have different properties from the random grain boundaries found in large grained nickel.

A negative deviation from the Hall–Petch law was also obtained by Abrahamson [42] in the case of steels

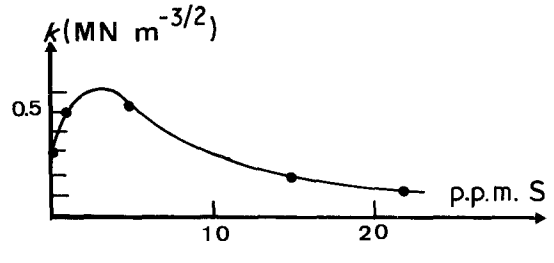

Figure 12 The dependence of the Hall–Petch parameter, k, on the sulphur content of pure nickel [24].

with a grain size smaller than 1 μm. According to Armstrong [43], this anomalous deviation might have an extrinsic origin: yielding in ultra-fine grain materials would initiate on microcracks or other stress concentration generators such as inclusions, holes or surface defects of a size now larger than the grain size itself. This interpretation seems reasonable since the more recent measurements of yield stress in fine-grained alloys do not exhibit any negative anomaly below 1 μm. For example, Taub *et al.* [22] found that the laboratory prepared RSR René 80 alloy obeyed the Hall–Petch law to 0.3 μm (Fig. 3b).

The suggestion that σ should be proportional to d^{-1} at small grain sizes due to the influence of the grain boundary zone [16] received no convincing experimental confirmation. Such a variation was effectively reported in aluminium alloys with grains smaller than 10 μm [44], but the $\sigma = Ad^{-1}$ relation was only true in the domain where deformation developed heterogeneously by Lüders bands. When the deformation was homogeneous the Hall–Petch relation was verified. The only perculiarity of the fine-grained alloys was that the slope k was almost independent of strain, in contrast with the large grained alloys. A feature that they share with the ODS alloys [32] where the strong obstacles are more closely spaced than the GB themselves. Microstructural observations confirmed that, for grain sizes below the micron range, the slip distance was equal to the grain diameter so that the grain interior was free of dislocations, even after a large plastic deformation.

In conclusion the Hall–Petch law seems to describe correctly the strengthening effect provided by the grain boundaries even for sizes smaller than 1 μm; however, the strain dependence of k vanishes at small sizes. Due to the lack of experimental results it is not yet possible to conclude whether or not there is a breakdown of the law below 0.1 μm as the pile-up model would suggest.

2.3.3. Ductility

A reduction in grain size can have several beneficial effects. It can delay crack nucleation and increase ductility by:

(a) reducing the slip length and therefore the stress concentrations

(b) reducing the importance of the Von Mises criterion: as multiple slip is usually fairly general in the vicinity of grain boundaries, the smaller the grain size, the more homogeneous the deformation.

The beneficial effect of a reduced grain size is illustrated in Fig. 13 by comparison of the ductility at low temperature ($< 700°$ C) between large-grained IN 738 and the same alloy obtained by plasma spraying ($d \simeq 2$ μm) [45]. A drastic increase in ductility can be obtained as a result of grain refinement in brittle materials, such as intermetallic compounds Ni_3Al [46] and NiAl [47] prepared by rapid solidification. The ductility of NiAl at 400° C is larger than 10% when $d < 20$ μm (Fig. 14).

In Ni_3Al with grain sizes smaller than 5 μm, elongations up to 30% were obtained at room temperature

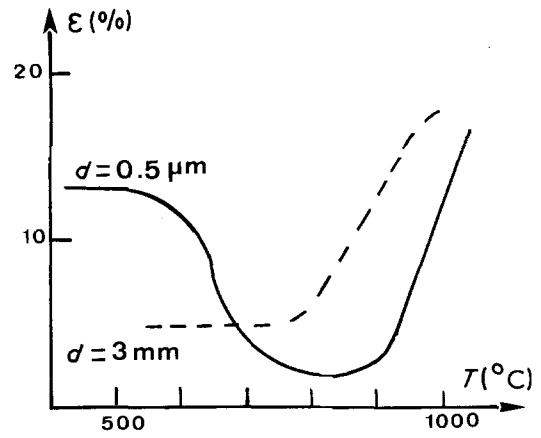

Figure 13 Ductility against temperature in fine grain and large grain IN 738 [45].

[26]. In the case of Ni_3Al several investigations [26, 48] have emphasized that for a given grain size, the ductility was also very sensitive to small additions of boron. As this element segregates to the grain boundaries, it can increase the resistance to intergranular crack propagation. It is also quite likely that some features of the structure after rapid quenching, the size of the anti-phase domain for instance, are very sensitive to composition. This can in turn have an influence on the ductility [49].

As discussed recently by Schulson [50], a material is ductile if the yield stress, as given by the Hall–Petch relation, is smaller than the stress sufficient to propagate a microcrack at length $2a = d$. This leads to the following condition for ductility

$$\sigma_0 + kd^{-1/2} < YK_{Ic}(2\pi a)^{-1/2} \quad (7)$$

where Y is a constant. A critical grain size, above which ductility is impaired can thus be defined as

$$d_c = Y'\left(\frac{K_{Ic} - k}{\sigma_0}\right)^2 \quad (8)$$

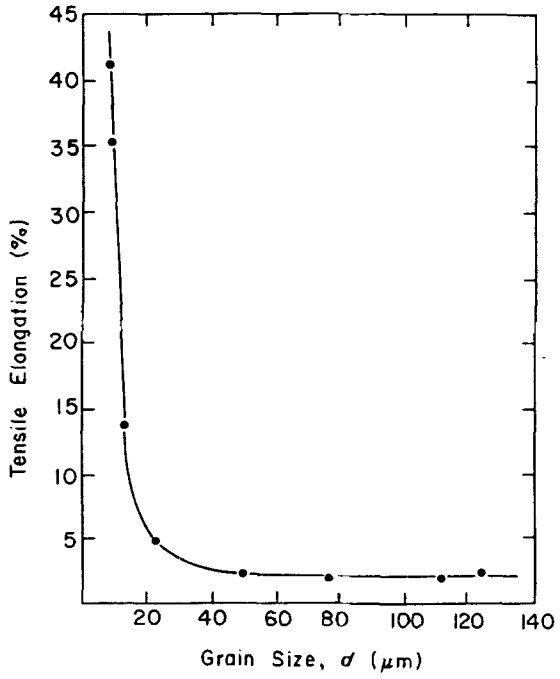

Figure 14 Elongation against grain size of $Ni_{51}Al_{44}$ deformed at 400° C with a strain rate of 1×10^{-4} sec^{-1} [47].

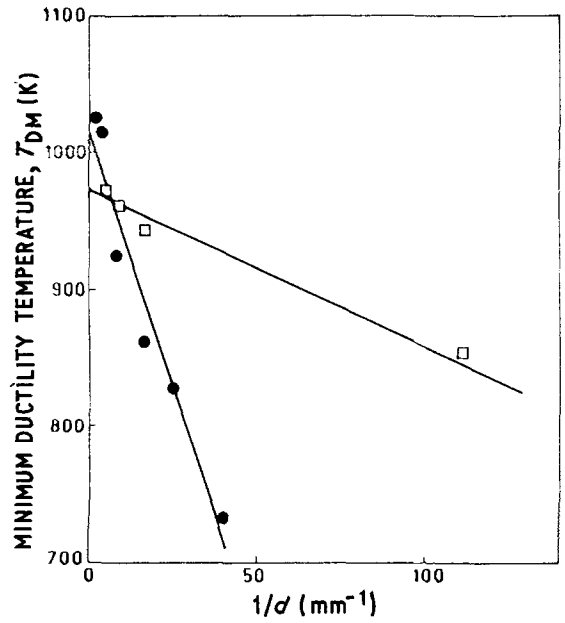

Figure 15 Variation in minimum ductility temperature, T_{DM}, with $1/d$: ● – AISI 316 steel, □ – Inconel X750 [52].

where $Y' \simeq 1$ is a geometrical parameter. A similar criterion was introduced years ago by Cottrell [51] in order to explain the shift in the ductile–brittle transition with grain size in carbon steels.

The application of this criterion to Ni-based superalloys where $K_{Ic} = 70\,\text{MPa}\,\text{m}^{-1/2}$ yields $d_c = 10\,\text{mm}$, a condition which is easily fulfilled in common practice. On the other hand, in brittle intermetallic materials such as Ni–Al, the critical grain size can be estimated at $d_c \simeq 50\,\mu\text{m}$ [47]. This rather small value could well explain why such very small grain sizes are required in order to ensure some ductility.

In austenitic stainless steel Mannan *et al.* [52] reported a sharp increase in ductility with grain size until an optimal value was reached around 100 μm at room temperature and around 200–300 μm at temperatures up to 850° C. The temperature of the ductility minimum, a feature common to most fcc alloys, was found to increase with increasing grain size (Fig. 15) and to correspond to the occurrence of intergranular fracture caused by a maximum of grain boundary sliding and a lack of stress-relieving mechanisms such as fast recovery or recrystallization.

3. Influence of grain size on the creep properties

3.1. Steady-state creep rate

When deformation occurs by slip and climb of dislocations, the creep rate is theoretically independent of grain size; however, we shall see later that a strengthening effect of the grain boundaries is frequently observed at low temperature and high stresses. On the other hand when recovery processes are activated, they are enhanced in the vicinity of the grain boundaries where subgrains larger than in the grain interior (Fig. 9b) are often observed at high temperature [34].

In all the mechanisms where a diffusional transport of atoms is involved the grain size is an important parameter. Two types of mechanisms are concerned:

TABLE III Creep mechanisms

Mechanisms	Equation for $\dot{\varepsilon}_s$ (sec^{-1})		Remarks
Dislocation climb	$\dot{\varepsilon}_s = AD\frac{Gb}{kT}\left(\frac{\sigma}{G}\right)^{4.5}$	(1)	$A \simeq 10^6$ G = shear modulus
Diffusional creep			
Nabarro–Herring (bulk)	$\dot{\varepsilon}_s = BD\frac{Gb}{kT}\left(\frac{b}{d}\right)^2\frac{\sigma}{G}$	(2a)	$B \simeq 30$ Threshold stress $\simeq 10^{-7}G$
Coble (grain boundaries)	$\dot{\varepsilon}_s = C\left(\frac{D_{GB}Gb}{kT}\right)\left(\frac{b}{d}\right)^3\frac{\sigma}{G}$	(2b)	$C \simeq 70$ Threshold stress $G\frac{b}{d}$
Ashby–Verrall (diffusion accommodated flow)	$\dot{\varepsilon} = FD\frac{b}{kT}\left(\frac{b}{d}\right)^2(\sigma - \sigma_1)\left[1 + \frac{\delta}{d}\left(\frac{D_{GB}}{D}\right)\right]$	(2c)	$F \simeq 100$ δ = GB thickness Threshold stress $\sigma_1 = \frac{0.7\Gamma}{d}$ Γ = GB free energy
GB sliding			
Controlled by GB diffusion	$\dot{\varepsilon}_s = HD_{GB}\frac{Gb}{kT}\left(\frac{b}{d}\right)^3\left(\frac{\sigma}{G}\right)^2$	(3a)	$H \simeq 8 \times 10^5$
Controlled by lattice diffusion	$\dot{\varepsilon}_s = LD\frac{Gb}{kT}\left(\frac{b}{d}\right)^2\left(\frac{\sigma}{G}\right)^2$	(3b)	$L \simeq 10^7$
Harper–Dorn	$\dot{\varepsilon} = MD\frac{Gb}{kT}\frac{\sigma}{G}$	(4)	$M \simeq 10^{-11}$

either purely diffusional mechanisms such as Nabarro–Herring and Coble creep or grain boundary sliding mechanisms. The creep rate is then a decreasing function of the grain size, $\varepsilon_s = Ad^{-n}$. If the diffusion path goes through the bulk of the grain then $n = 2$; if it involves the grain boundary area then $n = 3$. Some constitutive equations for creep are gathered in Table III.

When several independent processes are activated, the controlling mechanism is that giving the highest creep rate under the predetermined conditions of temperature, T, stress, σ, and grain size, d. At a given value of these three parameters, two-dimensional deformation maps can be drawn. The grain size is often chosen as a fixed parameter.

The first deformation maps were calculated by Ashby [53] in the σ–T plane. They were later refined to take into account the grain size [54, 55] and the various types of grain boundary sliding [56, 57].

Fig. 16 is an example of a normalized τ/G against T/T_m map for nickel with $d = 10\,\mu m$. In this case the deformation is controlled by GB diffusion or GB sliding in most of the experimental conditions. Fig. 17 is a normalized d/b against T/T_m map drawn for aluminium and is quite typical of fcc alloys with a high stacking fault energy. It shows that at grain sizes below $10^4\,b$ and for a normalized stress of 5×10^4, grain boundary sliding is controlling deformation in fcc materials.

The mechanical properties of metallic alloys with submicronic grain sizes are yet to be explored but much interest is devoted to them since they could be very attractive at intermediate temperatures ($T \simeq 0.5\,T_m$). In ceramic materials (MgO) for instance, Crampon and Escaig [58] could reach elongations of about 80% at 1000–1100° C on samples with 0.1 μm grain size in an otherwise very brittle material. Similar improvements might be achieved in metals and alloys since they seem to result from the extended domain where Coble creep is controlling deformation.

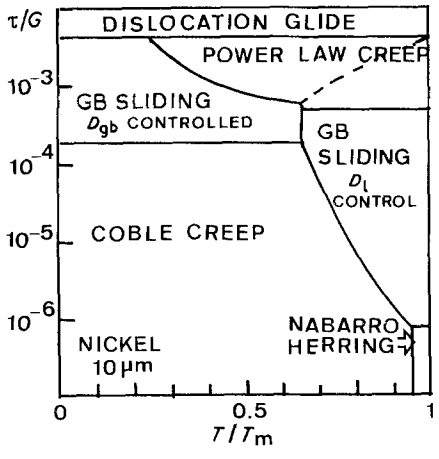

Figure 16 Normalized stress against temperature map for the deformation mechanism of nickel at $d = 10\,\mu m$ [56].

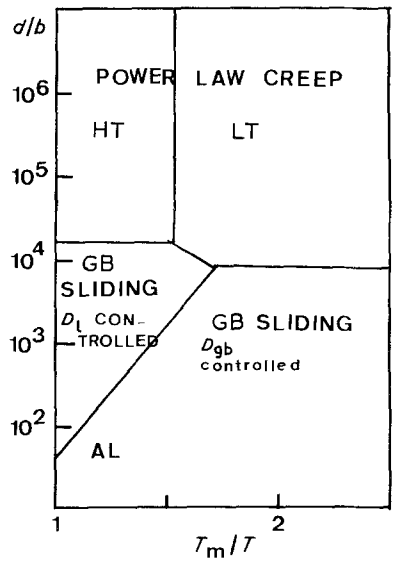

Figure 17 Normalized grain size against temperature map for $\tau = 5 \times 10^{-4}G$ in aluminium [56].

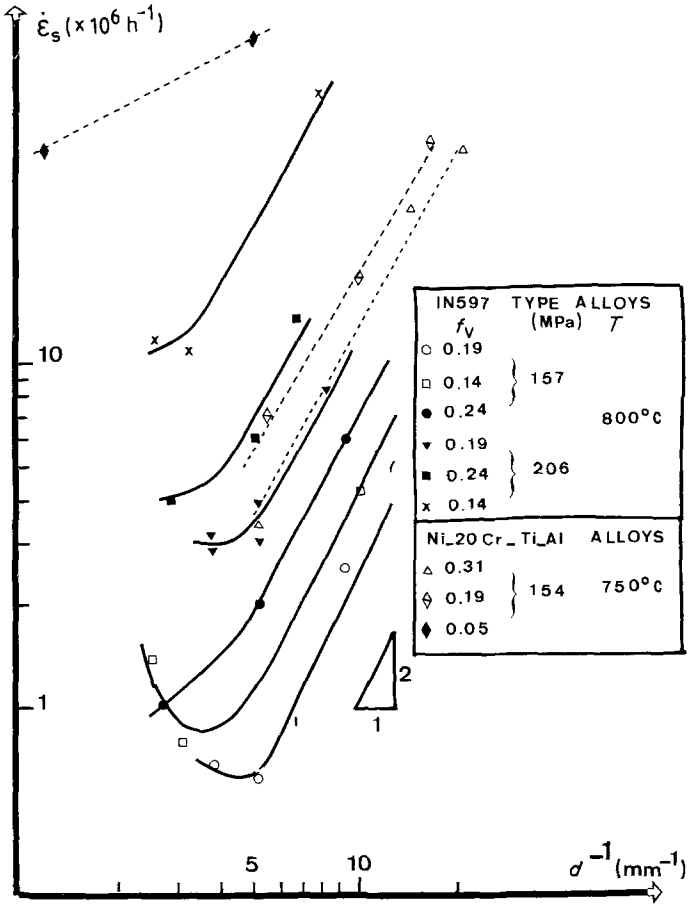

Figure 18 The effect of grain size on the minimum creep rate for a series of Ni-based alloys tested at 800° C [59].

3.1.1. Experimental results on Ni-based alloys

Above $0.5\,T_m$ the secondary creep rate in most superalloys is generally a decreasing function of d when $d < 100\,\mu m$. The lack of creep resistance of small grain materials is usually attributed to intense GB sliding. An example is given on Fig. 18 for a series of alloys containing various γ' volume fractions, f_v. At small grain sizes the steady-state creep rate $\dot{\varepsilon}_s$ is proportional to d^{-2} which indicates that the deformation rate is controlled by lattice diffusion [59].

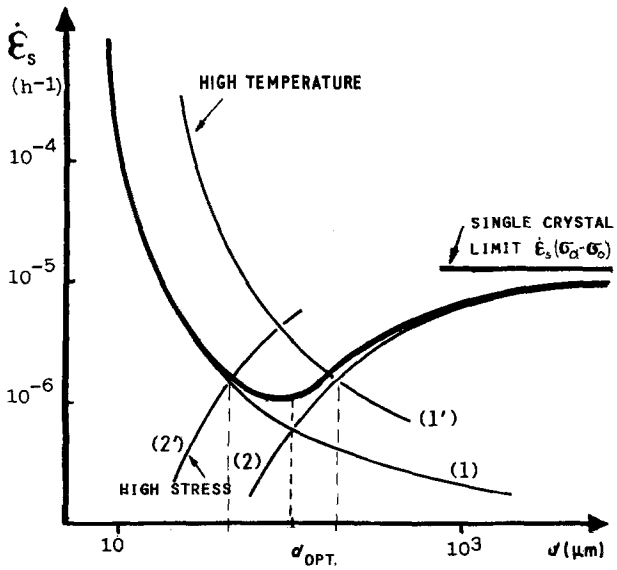

Figure 19 Existence of an optimal grain size for which the minimal creep rate $\dot{\varepsilon}_s$ is lowest. A schematic representation of Equation 11 in a superalloy with $f_v = 20\%$ tested at 800° C under 150 MPa, for instance.

According to the models a dislocation climb mechanism should become dominant above a critical grain size, d_c, and $\dot{\varepsilon}_s$ should then be independent of d (Table III). In fact, an optimal value of the grain size d_{opt} can be defined where $\dot{\varepsilon}_s$ is minimal as shown schematically on Fig. 19. This observation is quite general and has been reported in other metallic alloys [60]. It brings compelling evidence that both the strengthening effect of the grain boundary and its ability to act as a preferential path for deformation should be included in a complete description of the steady-state creep rate. As a first approach we can choose Expression 3b (Table III) in order to describe the contribution of the grain boundaries to the steady-state creep rate when σ_a is the applied stress, and add it to an expression similar to Equation 1 (Table III) for the description of the dislocation creep mechanism:

$$\dot{\varepsilon}_s = 10^7 D \frac{Gb}{k_0 T}\left(\frac{b}{d}\right)^2\left(\frac{\sigma_a}{G}\right)^2 + 10^6 D \frac{Gb}{k_0 T}\left(\frac{\sigma_e}{G}\right)^{4.5} \quad (9)$$

where D is the diffusion coefficient at temperature T, k_0 is Boltzmann's constant, $\sigma_e = \sigma_a - \sigma_i$ is the effective stress experienced by the dislocations and σ_i the internal stress inside the material. In second phase hardened alloys σ_i plays a major role in creep equations and can be related to the particle size and distribution [61, 62]. In order to include grain size effects as well, we suggest taking

$$\sigma_e = \sigma_a - \sigma_0 - kd^{-1/2} \quad (10)$$

where σ_0 is to be associated with microstructural hardening. Then Equation 9 becomes

$$\dot{\varepsilon}_s = 10^6 D \frac{Gb}{k_0 T}\left[10\left(\frac{b}{d}\right)^2\left(\frac{\sigma_a}{G}\right)^2 + \left(\frac{\sigma_a - \sigma_0 - kd^{-1/2}}{G}\right)^{4.5}\right] \quad (11)$$

These two contributions can be represented separately by Curve 1 (Fig. 19) with $\dot{\varepsilon}_s$ decreasing rapidly as the grain size is increased (d^{-2}), and Curve 2 describing the slowly growing contribution of the intragranular phenomena to the general plastic flow of the material as grains become larger ($-d^{-1/2}$). This latter contribution saturates as d goes to infinity and $\dot{\varepsilon}_s$ tends toward the creep rate for a single crystal under an effective stress[9] ($\sigma_a - \sigma_0$). In former models [60] containing a term proportional to d^2, the creep of large grain or single crystal materials could not be adequately described. With this approach, an optimal grain size of

$$d_{opt} = 4\left[\frac{G(b)^{1/2}}{k}\right]^{2/3}\left(\frac{\sigma_a}{\sigma_e}\right)^{4/3}\left(\frac{Gb}{\sigma_e}\right) \quad (12)$$

can be derived from Equation 11 by looking for the value of d which ensures

$$\frac{\partial \dot{\varepsilon}_s}{\partial d} = 0$$

Taking the value of k for nickel from Table II and $\sigma_e = 0.2\sigma_a$ for an applied stress of $10^{-3}G$, yields $d_{opt} = 5 \times 10^5 b \simeq 100\,\mu m$ a value in good agreement with Fig. 18 and other results [60, 61, 63, 64]. For a given internal microstructure of a two-phase alloy σ_0 is constant and at:

a *high applied stress* $\sigma_a \gg \sigma_i$ then $\sigma_a/\sigma_e \simeq 1$ and d_{opt} is smaller (Fig. 19): smaller grain sizes are preferred at intermediate temperature under high loads.

a *low applied stress* $\sigma_a \simeq \sigma_i$ then $\sigma_a/\sigma_e \gg 1$, the value of d_{opt} increases. This is usually the case at high temperature (0.8 to 0.95 T_m) where creep stresses below the yield stress are usual and larger grain sizes ensure better creep resistance.

At very high temperatures, as in turbine blades for instance, $\dot{\varepsilon}_s$ for the single crystal, with an optimal distribution of the hardening phase, may be so low that the single crystal becomes the solution providing the highest creep resistance. In other words, taking full advantage of the internal strengthening mechanisms and the fine grain structure is only possible at low temperatures where the strength of the grain and of the boundaries lie in the same range. At high temperatures, the high creep resistance brought to the matrix by oxides, carbides, and/or precipitates cannot usually be matched by that of grain boundaries. Even in single-phase alloys such as 316-type stainless steels (Fig. 20) this model seems to describe rather well the region of the optimal size and of the large grain sizes, which has been explored recently by Mannan and Rodriguez [64].

In Ni-based superalloys, at grain sizes smaller than 10 μm, superplastic behaviour can be obtained at a temperature between 0.5 T_m and the γ' solvus. The gatorizing process (registered by the PWA corporation) is a method for obtaining superalloys with a small grain size ($d \simeq 1\,\mu m$) suitable for superplastic deformation. Superplastic behaviour was demonstrated in a number of superalloys such as, for instance IN 100 [65, 66] and MAR M 200 [67]. The role of GB sliding during superplastic deformation has been firmly established by Gifkins [68] in a number of alloys.

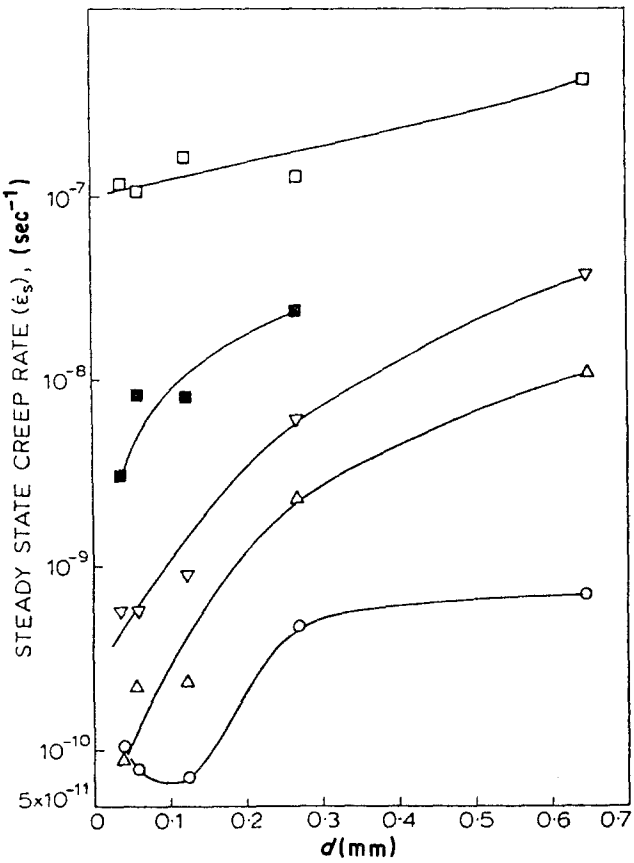

Figure 20 Variation of the steady-state creep rate $\dot{\varepsilon}_s$ with grain size for various stresses at 600° C in a 316-type stainless steel (d is the grain diameter) [64]. Stress (MNm^{-2}): (□) 260, (■) 220, (▽) 200, (△) 180, (○) 150.

Superplasticity was always observed when the following conditions were fulfilled: the grain must be fine and equiaxed, the volume fraction $f_v(\gamma')$ high enough so that the microstructure is stable above 0.5 T_m; the strain rate sensitivity $m = d(\log \sigma)/d(\log \dot{\varepsilon}_s)$ is generally around 0.5. Although $m = 0.5$ is coherent with a GB sliding mechanism, microstructural studies led to the conclusion that the deformation process was complex with several mechanisms occurring simultaneously [69]. This experimentally measured contribution of GB sliding is often found to reach 50% of the superplastic deformation. It means that superplasticity is generally encountered in conditions where GB sliding and grain deformation by dislocation glide occur simultaneously. This is possible in a limited range of strain rates usually between 10^{-3} and 10^{-1} sec^{-1}; the superplastic domain tends to drift to higher rates when d decreases.

3.2. Influence of geometrical factors

3.2.1. Shape of the grains

The theoretical creep rates given by the equations gathered in Table III are valid for equiaxed grains.

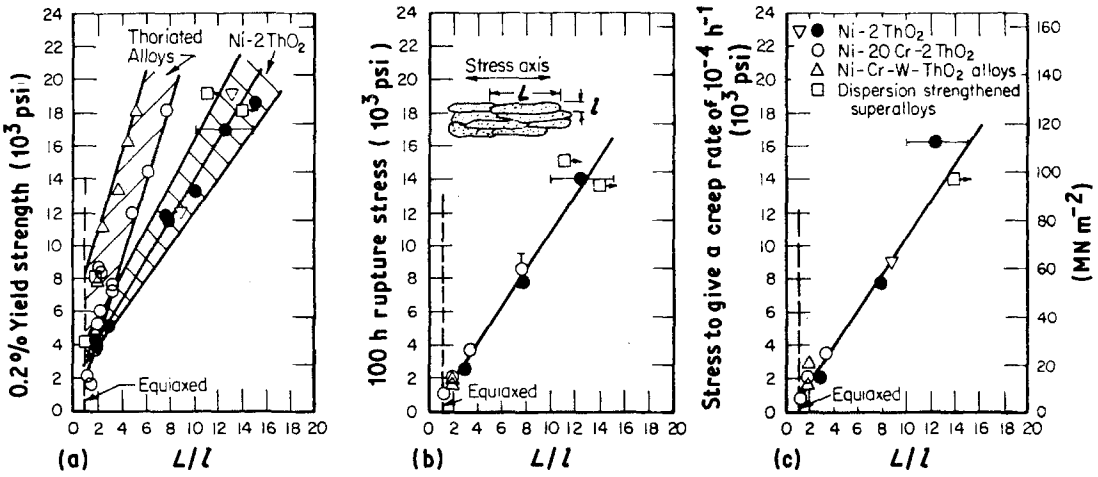

Figure 21 The effect of grain aspect ratio L/l, in dispersion strengthened nickel alloys on strength properties at 1093° C: (a) 0.2% offset yield strength; (b) 100 h rupture stress; (c) stress to give a minimum creep rate at 10^{-4} h^{-1}. Open points are recrystallized and closed points are non-recrystallized alloys [18].

When the grains are elongated parallel to the applied stress, an important fraction of the GB area is not exposed to any significant stress, the contribution of GB sliding to the deformation process is then reduced. Wilcox and Clauer [25] have shown that, in dispersed-phase alloys with elongated grains there was no relation between the high temperature strength and the transverse grain size. The mechanical strength was in fact an increasing function of the grain aspect ratio (GAR = L/l). Fig. 21 illustrates the drastic influence of the GAR on the strength at 1093° C in thoriated nickel.

Elongated grains are thus expected to give better strength above 0.5 T_m than equiaxed grains. Such a microstructure can be obtained, either by appropriate thermo-mechanical treatments such as hot extrusion and directional recrystallization in ODS alloys, or by directional solidification in the case of γ–γ' nickel alloys.

More recently Arzt and Singer [70] have illustrated the beneficial contribution to creep properties of factors such as elongated grain shape, boundary waviness and oxide dispersion strengthening. They showed that together with an improved rupture life, a transition from intergranular to transgranular fracture was observed (Fig. 22) on Iconel MA 6000 alloy when the GAR exceeded a critical value of about 20, and interpreted it as an effect of creep damage accumulation in longitudinal grain boundaries.

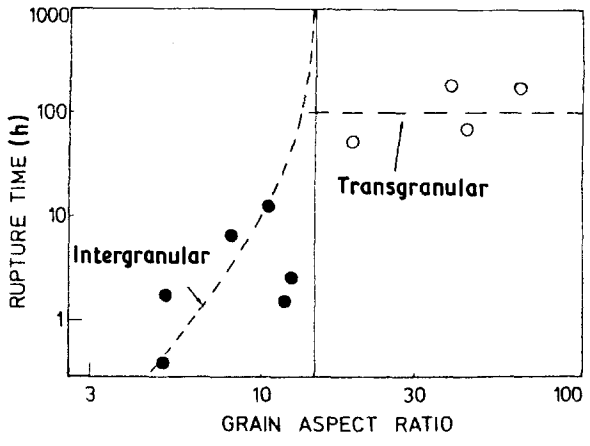

Figure 22 Change of fracture mode with GAR in MA 6000 nickel alloy creep tested at 950° C under 230 MNm^{-2} [70].

3.2.2. Structure of the grain boundaries

GB sliding can be reduced by introduction of anchoring obstacles within the boundary. Among the most potent obstacles let us mention carbides and serrated grain boundaries. An example of the improvement of creep resistance by GB carbides in Nimonic 115 is given in Fig. 23. Furillo *et al.* [71] showed that it was possible to reduce the amount of GB sliding during high temperature creep by increasing the volume fraction of $M_{23}C_6$ carbides in the grain boundaries. However, from these results it is not possible to decide whether the introduction of GB carbides completely inhibited GB sliding or whether it altered the deformation process into a dislocation creep mechanism.

The improvement of creep rupture life due to serrations on grain boundaries is well known (Fig. 24), these serrations should make GB sliding more difficult and increase the path for GB diffusion. However, their influence was studied mostly in pre-cracked samples [72] and will be described in the next section.

3.3. Effect of grain size on high temperature crack growth

Crack growth behaviour has received increasing attention in recent years since it determines the failure of high temperature industrial alloys. The time-dependent crack growth in the creep range is not fully understood, a review of the main models is given by Sadananda and Shahinian [73]. It is likely that, in most cases, crack growth occurs by a coupled diffusion–deformation mechanism. Several models correlate the crack growth rate da/dt to creep rate [74, 75], so that under the experimental conditions where GB sliding is dominant da/dt is proportional to d^{-n} in a way similar to the steady-state creep rate, $\dot{\varepsilon}_s$. Thus, the creep rupture strength improves when d increases. An example in alloy IN 792 is shown in

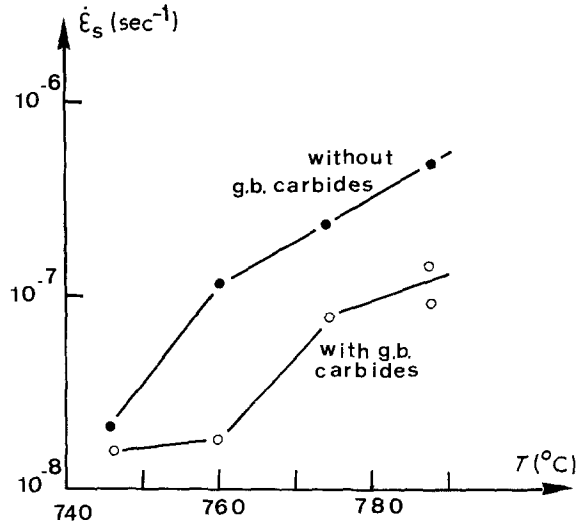

Figure 23 Influence of grain boundary carbides on the creep rate of Nimonic 115 [71]. σ = 517 MPa, d = 75 μm.

Fig. 25; the value of the initial stress intensity necessary to produce failure in 100 h at 704° C is plotted as a function of grain size [72]. Also in IN 792, the higher creep crack growth resistance obtained with serrated grain boundaries is clearly stigmatized on Fig. 24. These results in IN 792 are consistent with the model of Floreen and Kane [75]: in this model fracture propagates when the local strain ahead of the crack tip reaches a critical value, ε_c. In a number of Ni-based superalloys, the stress intensity to produce failure during creep can be expressed as:

$$K = |3EY\delta_0 + 0.3EY\varepsilon_c d|^{1/2} \quad (13)$$

where E is Young's modulus, Y the yield strength, δ_0 the crack opening displacement, and d the grain size. ε_c depends on the shape of the grain boundary, it takes on a value of 0.1 for smooth grain boundaries and 0.3 for serrated grain boundaries.

In conclusion grain refinement reduces the creep life of superalloys by increasing at the same time the secondary creep rate and the crack growth rate. This effect, illustrated by the results on IN 100 given in Fig. 26, is aggravated at high temperature.

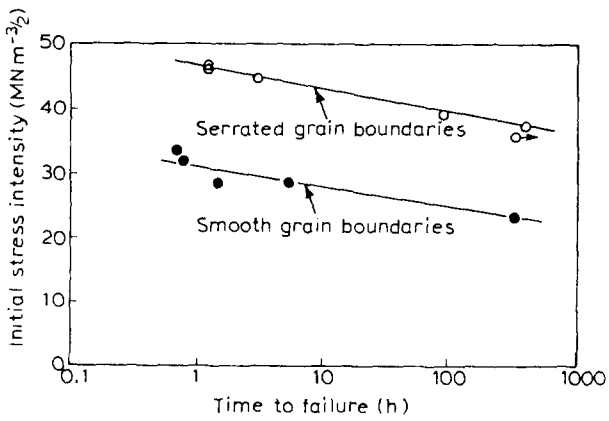

Figure 24 Time to failure at 704° C against initial intensity for a heat of IN 792 with either smooth or serrated grain boundaries [72].

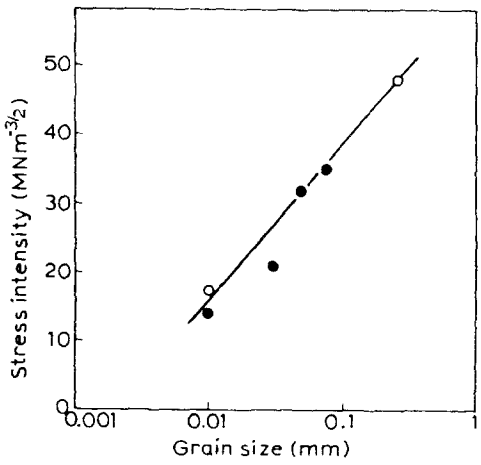

Figure 25 Value of initial stress intensity to produce failure in 100 h at 704° C against grain size IN 792 [72]. (○) Cast and wrought, (●) extruded powder.

4. Cyclic deformation at room temperature

A reduction in grain size has opposite effects on crack nucleation and crack propagation. Indeed, a small grain size promotes a more homogeneous deformation: this effect is known to retard crack nucleation by reducing stress concentrations. The influence of grain size on crack initiation is thus expected to be highest in alloys with a tendency for heterogeneous deformation, i.e. alloys with shearable precipitates and solid solutions with a low stacking fault energy. In PM Ni-based alloys the number of cycles for nucleation is increased by one order of magnitude when going from 180 to 70 μm sized powders [77]. Similarly in aluminium alloys containing shearable precipitates, the detrimental effect of precipitate free zones is reduced at small grain sizes [78] due to the smaller slip length, the same effect is expected in γ' hardened nickel alloys. On the contrary, as shown in Fe–Ni [79] it seems that fatigue cracks grow more quickly as the tendency for homogeneous slip is more pronounced. The growth rate, da/dN, of the fatigue cracks is usually expressed as a function of the alternating stress intensity ΔK. In a logarithmic plot the da/dN against ΔK curve is sigmoidal in shape with three stages (Fig. 27): Stage A

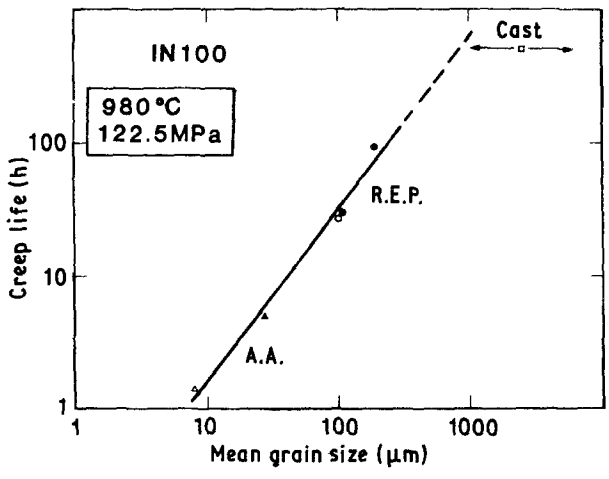

Figure 26 Effect of grain size on creep strength of IN 100 [76]. 980° C, 122.5 MPa. (□, ○, △) [27], (●, ▲) [39].

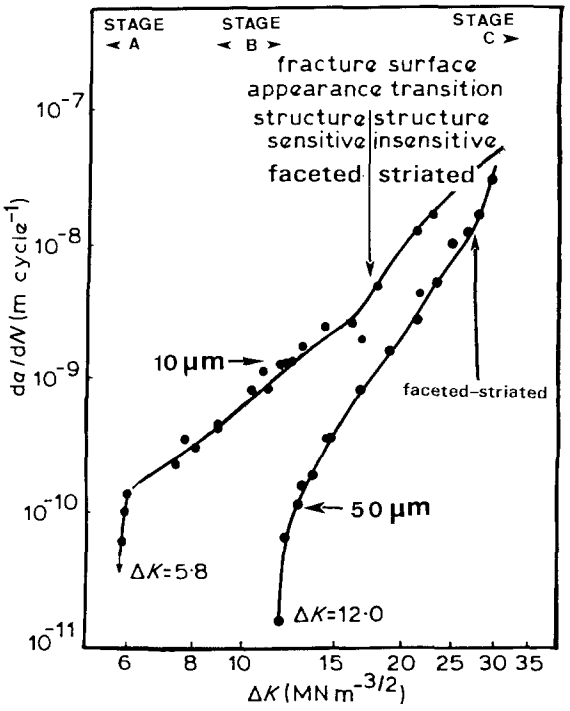

Figure 27 Influence of grain size on crack propagation rate and threshold in Nimonic AP1 [80].

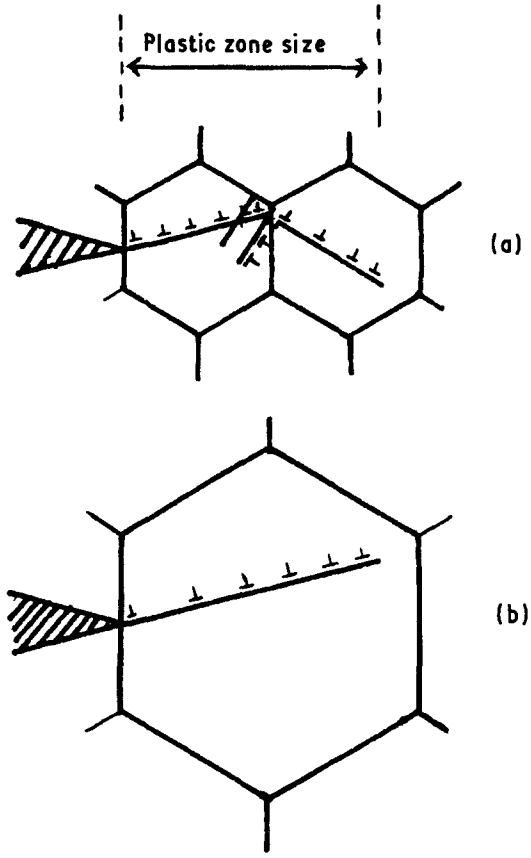

Figure 28 Interaction between grain size and the dislocation structure at the tip of the crack in (a) small grain material and (b) large grains [85].

near the threshold ΔK_{th} and Stage C near the final rupture are very sensitive to the microstructure and especially to grain size. Experimental results are often difficult to interpret because of the cumulative influences of grain size on one hand and of microstructural features such as the size and volume fraction of precipitates on the other. For instance, in a γ'-hardened alloy such as Waspaloy, an increase in grain size is equivalent to a decrease in precipitate size [81].

The threshold ΔK_{IC} seems to decrease significantly with d as shown in Fig. 27 for Nimonic AP1 (a Ni-based alloy with 45% γ'): ΔK_{IC} drops down from $12\,MNm^{-3/2}$ for $d = 50\,\mu m$ to $6\,MNm^{-3/2}$ for $d = 10\,\mu m$ [80]. However, in many Ni-based alloys [62, 82] near-threshold crack growth proceeds by propagation along slip bands. The sharp changes in the crack path that takes place when reaching grain boundaries produce rough fracture surfaces especially in materials with larger grain sizes. Venables *et al.* [83] recently pointed out that the shift in the threshold value with grain size was observed only in Astroloy for large load ratios (0.8) when crack closure problems may take place on rough surfaces. The effect of grain size on the propagation threshold should thus be considered as indirect.

In a pure fcc metal such as copper, the effect of grain size is very small and conflicting results are reported by Lukas and Kung [84] who seem to observe a $d^{1/2}$ dependence of ΔK crack propagation threshold ΔK_{th} whereas Higo *et al.* [31] suggest a relation such as

$$\Delta K_{th} = A + Bd^{-1/2} \qquad (14)$$

in pure copper as well as in Cu–Al alloys, where both A and B increase with increasing aluminium content, i.e. with decreasing SFE and more planar-type plastic deformation.

Although results are too scarce to allow definite conclusions it seems that the sensibility of the crack growth rate to grain size decreases when the γ' volume fraction of precipitates goes down: in Waspaloy where the volume fraction is of the order of 25%, the shift of the da/dN against ΔK curve when the grain size goes from 15 to 120 μm is apparently much smaller than in Nimonic AP1 with 45% volume fraction γ'.

All the results obtained in nickel alloys agree with those found in aluminium or titanium alloys [74, 85] and in steels [86]. The rationale for the observed effect is based on the comparison between the grain size and the radius of the reverse plastic deformation zone, $R \simeq 0.05(\Delta T/\sigma_y)^2$. As suggested by Hornbogen and Zum Gahr [79] and by Lindigkeit *et al.* [85], a reverse slip of the dislocations during unloading is possible if $R < d$ so that the accumulation of damage is small during cycling; however at small grain sizes ($d < R$), dislocations are trapped by grain boundaries on secondary slip systems. This reduction in the number of backward moving dislocations (Fig. 28) causes an accumulation of damage.

As the radius of the plastic zone increases with ΔK a transition from a large grain size behaviour to a fine grain size behaviour can be expected in alloys with a medium grain size. According to King [80], this is the case in a number of Ni-based, Fe-based and Ti-based alloys. At the transition, a step is observed in the da/dN against ΔK curve and there is a change from a faceted crystallographic fracture mode to a striated fracture surface (Fig. 27).

Acknowledgements

The authors would like to thank ONERA and the Ecole des Mines de Paris for financial support. Thanks are also due to Professor R. W. Cahn who kindly suggested this review work and renewed his encouragement until its completion.

References

1. V. KUTUMBA RAO, D. M. R. TAPLIN and P. R. RAO, *Met. Trans.* **6A** (1975) 77.
2. T. B. GIBBONS and B. E. HOPKINS, *Met. Sci.* **5** (1971) 233.
3. R. W. CAHN, *Ann. Rev. Mater. Sci.* **12** (1982) 51.
4. E. O. HALL, *Proc. Phys. Soc. (London)* **B64** (1951) 747.
5. N. J. PETCH, *J. Iron Steel Inst.* **174** (1953) 25.
6. J. C. M. LI and Y. T. CHOU, *Met. Trans.* **1** (1970) 1145.
7. R. W. ARMSTRONG, "Yield, Flow and Fracture of Polycrystals", edited by T. N. Baker (Applied Science, Cambridge, 1983) p. 1.
8. A. H. COTTRELL, *Trans. TMS AIME* **212** (1958) 192.
9. J. C. M. LI and G. C. T. LIU, *Phil. Mag.* **38** (1967) 1059.
10. R. ARMSTRONG, I. CODD, R. M. DOUTHWAITE and N. J. PETCH, *ibid.* **7** (1962) 45.
11. J. D. MEAKIN and N. J. PETCH, Symposium on the Role of Substructure in the Mechanical Behaviour of Metals, Air Force Systems Command, ASD TDR 63-234, Orlando, FL, April (1963) p. 243.
12. M. F. ASHBY, *Phil. Mag.* **21** (1970) 399.
13. A. W. THOMPSON, M. I. BASKES and W. F. FLANAGAN, *Acta Metall.* **21** (1973) 1017.
14. J. C. M. LI, *J. Appl. Phys.* **32** (1961) 525.
15. *Idem, Trans. TMS AIME* **227** (1963) 247.
16. U. F. KOCKS, *Met. Trans.* **1** (1970) 1121.
17. D. E. SONON and G. V. SMITH, *Trans. AIME* **242** (1968) 1527.
18. B. A. WILCOX and A. H. CLAUER, *Acta Metall.* **20** (1972) 743.
19. Y. NAKADA and A. S. KEH, *Met. Trans.* **2** (1971) 441.
20. A. W. THOMPSON, *Acta Metall.* **23** (1975) 1337.
21. R. D. CARNAHAN and J. E. WHITE, *Phil. Mag.* **10** (1964) 513.
22. A. I. TAUB, M. R. JACKSON, S. C. HUANG and E. L. HALL, "Rapidly Solidified Metastable Materials" edited by B. H. Kear and B. C. Giessen (Elsevier, Amsterdam, 1984) p. 389.
23. A. W. THOMPSON, *Acta Metall.* **25** (1977) 83.
24. S. FLOREEN and J. H. WESTBROOK, *ibid.* **17** (1969) 1175.
25. B. A. WILCOX and A. H. CLAUER, "The Superalloys" edited by C. T. Sims and W. C. Hagel (John Wiley, Chichester, 1972) p. 197.
26. A. J. TAUB, S. C. HUANG and K. M. CHANG, *Met. Trans.* **15A** (1984) 399.
27. M. KUHLMEYER, Proceedings of ICSMA 5, edited by A. Haasen *et al.* (Pergamon, Oxford, 1979) p. 855.
28. E. WERNER and H. P. STÜWE, *Mater. Sci. Eng.* **68** (1985) 175.
29. J. WERT, Proceedings of ISCMA 6, Melbourne (1982), edited by R. C. Gifkins (Pergamon) p. 339.
30. Y. W. KIM and W. M. GRIFFITH, "PM Aerospace Materials" (Bern, 1984) Metal Powder Report (1985) Vol. 1, p. 33.
31. Y. HIGO, A. C. PIKARD and J. F. KNOTT, *Met. Sci.* **15** (1981) 233.
32. N. HANSEN, "Yield, Flow and Fracture of Polycrystals" edited by T. N. Baker (Applied Science, Cambridge, 1983) p. 311.
33. C. Y. BARLOW, A. J. PORTER and B. RALPH, Proceedings of the 2nd RISØ International Symposium, edited by N. Hansen, A. Hoisewell, T. Liffins and H. Lilholt (RISØ, 1981) p. 131.
34. D. McLEAN, Proceedings of ICSMA 4, Nancy 1976 (Laboratoire de physique du solide EMSMIH, Nancy) Vol. 3, p. 958.
35. V. V. KARAEVA and V. F. SAKHOVAROV, *Izv. Vyssl. Ycheb. Zaved* **5** (1965) 40.
36. D. V. WILSON, *Met. Sci.* **1** (1967) 40.
37. L. E. MURR, *Mater. Sci. Eng.* **51** (1981) 71.
38. A. MASCANZONI and G. BUZZICHELLI, *Phil. Mag.* **22** (1970) 857.
39. E. VENKASTESH and L. E. MURR, *Mater. Sci. Eng.* **33** (1978) 69.
40. J. M. BERNSTEIN and B. B. RATH, *Surf. Sci.* **31** (1972) 97.
41. L. A. DAVIS, "Metallic Glasses" (ASM Metals Park, Ohio, 1978) p. 190.
42. E. P. ABRAHAMSON, "Surfaces and Interfaces II" edited by A. Burke *et al.* (Syracuse University Press, New York, 1968) p. 262.
43. R. W. ARMSTRONG, Proceedings of ISCMA 5, edited by P. Haasen, V. Gerold and G. Kostorz (Pergamon Press, Oxford, 1979) p. 795.
44. D. J. LLOYD, *Mater. Sci.* **14** (1980) 193.
45. M. R. JACKSON, J. R. RAIRDEN, J. S. SMITH and R. W. SMITH, *J. Metals* **33** (1981) 23.
46. A. INOUE, H. TAMIOKA and T. MASUMOTO, *J. Mater. Sci. Lett.* **1** (1982) 377.
47. E. SCHULSON and D. R. BARKER, *Scripta Metall.* **17** (1983) 519.
48. K. AOKI and O. IZUMI, *J. Jpn Inst. Met.* **43** (1979) 1190.
49. A. INOUE, H. TOMIOKA and T. MASUMOTO, *Met. Trans.* **14A** (1983) 1367.
50. E. M. SCHULSON, *Res. Mech. Lett.* **1** (1981) 111.
51. A. H. COTTRELL, *Trans. AIME* **212** (1958) 192.
52. S. L. MANNAN, K. G. SAMUEL and P. RODRIGUEZ, *Mater. Sci. Eng.* **68** (1985) 143.
53. M. F. ASHBY, *Acta Metall.* **20** (1972) 887.
54. F. A. MOHAMED and T. G. LANGDON, *Met. Trans.* **5** (1974) 2339.
55. *Idem, J. Eng. Mater. Technol.* **98** (1976) 125.
56. A. LUHY, R. A. WHITE and O. D. SHERBY, *Mater. Sci. Eng.* **39** (1979) 211.
57. O. A. RUANO and O. D. SHERBY, *ibid.* **56** (1982) 167.
58. J. CRAMPON and B. ESCAIG, *J. Amer. Ceram. Soc.* **63** (1980) 680.
59. V. LUPINC and T. B. GIBBONS, "High Temperature Alloys for Gas Turbines", edited by D. Coutsouradis, P. Felix, H. Fischmeister, L. Habraken, Y. Lindblom and M. O. Speidel (Applied Science, 1978) p. 335.
60. F. GAROFALO, "Fundamentals of Creep and Creep Rupture in Metals" (Macmillan, London, 1965) p. 27.
61. J. P. DENISSON, P. D. HOLMES and B. WILSHIRE, *Mater. Sci. Eng.* **33** (1978) 35.
62. J. N. VINCENT and L. REMY, Advances in Fracture Research, 1984, Proceedings of ICF6, edited by S. R. Valluri, D. H. R. Taplin, P. Rama Rao, J. F. Knott and R. Dubey (Pergamon, 1985) Vol. 4, p. 2513.
63. C. CARRY and J. L. STRUDEL, *Acta Metall.* **26** (1978) 859.
64. S. L. MANNAN and P. RODRIGUEZ, *Met. Sci.* **17** (1983) 63.
65. S. H. REICHMAN and J. W. SMITH, *Int. J. Powder Met.* **6** (1970) 65.
66. R. G. MENZIES, G. H. DAVIES and J. W. EDINGTON, *Met. Sci.* **16** (1982) 356.
67. J. P. A. IMMARIGEON and P. H. FLOYD, *Met. Trans.* **12A** (1981) 1177.
68. R. C. GIFKINS, *ibid.* **7A** (1976) 1225.
69. J. W. EDINGTON, *ibid.* **13A** (1982) 703.
70. E. ARZT and R. F. SINGER, "Superalloys 1984" edited by M. Gell, C. S. Kortovich, W. B. Kent and J. F. Radavich, (AIME Conference Proceedings, 1984) p. 367.
71. F. T. FURILLO, J. M. DAVIDSON and J. K. TIEN, *Mater. Sci. Eng.* **39** (1979) 267.
72. J. M. LARSON and S. FLOREEN, *Met. Trans.* **8A** (1977) 51.

73. K. SADANANDA and P. SHAHINIAN, *Met. Sci.* **15** (1981) 425.
74. J. T. BARNBY, *Eng. Fract. Mech.* **7** (1975) 299.
75. S. FLOREEN and R. H. KANE, *Met. Trans.* **7A** (1976) 1157.
76. J. H. DAVIDSON and C. AUBIN, "High Temperature Alloys for Gas Turbines", edited by A. Brunetaud *et al.* (Reidel, New York, 1982) p. 853.
77. F. L. VERSNYDER, *ibid.*, p. 33.
78. E. A. STARKE Jr and G. LUTJERING, Proceedings of the ASM Seminar on Materials Science Fatigue and Microstructure, October 1978, St. Louis, Missouri (ASM, Metals Park, Ohio, 1978) p. 205.
79. E. HORNBOGEN and K. H. ZUM GAHR, *Acta Metall.* **24** (1970) 581.
80. J. E. KING, *Met. Sci.* **16** (1982) 345.
81. B. A. LERCH, N. JAYARAMAN and S. D. ANTOLOVICH, *Mater. Sci. Eng.* **16** (1982) 345.
82. M. A. HICKS and J. E. KING, *Int. J. Fatigue* **5** (1983) 67.
83. R. A. VENABLES, M. A. HICKS and J. E. KING, Fatigue Crack Growth – Threshold Concepts, ASM Fall Meeting, Philadelphia (1983) edited by D. L. Davidson and S. Surech (Metallurgical Society AIME, 1983) p. 341.
84. P. LUKAS and L. KUNG, *Mater. Sci. Eng.* **62** (1984) 149.
85. J. LINDIGKEIT, G. TERLINDE, A. GYSLER and G. LUTZERING, *Acta Metall.* **27** (1979) 1717.
86. R. O. RITCHIE, *Met. Sci.* **11** (1977) 368.

Received 5 June
and accepted 10 July 1985